nature biotechnology

A molecular ruler based on plasmon coupling of single gold and silver nanoparticles

Carsten Sönnichsen[1,3], Björn M Reinhard[2,3], Jan Liphardt[2] & A Paul Alivisatos[1]

Förster Resonance Energy Transfer has served as a molecular ruler that reports conformational changes and intramolecular distances of single biomolecules[1–4]. However, such rulers suffer from low and fluctuating signal intensities, limited observation time due to photobleaching, and an upper distance limit of ~10 nm. Noble metal nanoparticles have plasmon resonances in the visible range and do not blink or bleach. They have been employed as alternative probes to overcome the limitations of organic fluorophores[5,6], and the coupling of plasmons in nearby particles has been exploited to detect particle aggregation by a distinct color change in bulk experiments[7–9]. Here we demonstrate that plasmon coupling can be used to monitor distances between single pairs of gold and silver nanoparticles. We followed the directed assembly of gold and silver nanoparticle dimers in real time and studied the kinetics of single DNA hybridization events. These 'plasmon rulers' allowed us to continuously monitor separations of up to 70 nm for >3,000 s.

The optical properties of colloidal gold have been studied for over 100 years[10,11]. The discovery of surface-enhanced Raman scattering of molecules near metal structures has renewed interest in plasmon resonances of metal particles[12]. Functionalized metal particles are currently being used to detect biomolecules with up to zeptomole sensitivity in bulk experiments[7,8,13]. Moreover, the binding of proteins to single functionalized particles can be followed by darkfield microscopy, by exploiting the dependence of the plasmon resonance wavelength on the refractive index of the particle's surroundings[14,15]. The plasmon resonance wavelength of a metal nanoparticle is also affected by other nanoparticles that are in its immediate environment. When two nanoparticles are brought into proximity, their plasmons couple, which shifts the resonance wavelength depending on the particle separation. Since this effect is well-known theoretically[16,17] and observed experimentally for fixed distances[18,19], we sought to explore its use as a molecular ruler. We applied 'plasmon rulers' to study the dynamics of DNA hybridization on the single-molecule level. DNA was chosen as our model system for four reasons: (i) DNA has been used successfully to assemble discrete nanostructures[20,21]; (ii) plasmon coupling has been shown in bulk experiments to detect specific DNA targets[7,13]; (iii) the length of DNA can be readily chosen and controlled and is well understood[22]; (iv) the kinetics of single DNA molecule hybridization is relevant for biotechnology and nanoscience applications[23,24].

We used gold and silver nanoparticles 40 nm in diameter. The diameter was chosen to ensure a sufficiently intense light-scattering signal while minimizing any effects of the particles on proximal biomolecules. However, we found that a reduction in particle size to 20 nm for silver and 30 nm for gold is possible with the current technique. Particles were illuminated with unpolarized white light, and light scattered by individual particles was collected by a darkfield microscope in transmission mode (**Fig. 1a**)[25]. Upon introduction of streptavidin-functionalized particles into the bovine serum albumin (BSA)-biotin–coated glass chamber, we immediately observed numerous scattering sources adhering to the chamber surfaces. Nanoparticles were vividly colored: individual silver nanoparticles were blue (**Fig. 1b**); gold nanoparticles were green (**Fig. 1c**); aggregates were red-shifted compared to individual particles (typically by about 50 nm for gold, 150 nm for silver); and dust and scratches were white.

Our first application of plasmon coupling was to monitor the directed assembly of functionalized particle pairs. We used surface-immobilized particles (**Fig. 1b,c**) as anchors for single-stranded DNA (ssDNA)-functionalized particles. The 33-nucleotide ssDNA molecules had a biotin at their 3′ end, allowing them to bind to the streptavidin-coated anchor particles (**Fig. 1a**). After the ssDNA-functionalized particles were introduced into the chamber, some scattering centers suddenly changed color owing to dimer formation. Silver particles turned from blue to green (**Fig. 1b**); gold particles turned from green to orange (**Fig. 1c**). The spectral shift upon dimer formation was considerably larger for silver particles (102 nm) than for gold particles (23 nm, **Fig. 1d**). The fraction of surface-immobilized particles that captured a ssDNA-functionalized particle ranged from 10–86% depending on the time the samples had been stored, with fresher particles performing better. Aggregates of more than two particles were easily identified by their intensity and distinct color, with multiple peaks in the spectrum (see for example the purple dot in **Fig. 1b**). To prevent the formation of such aggregates in subsequent experiments, we adjusted the incubation time and particle concentration until $<10\%$ of the surface-immobilized particles were involved in coupling events. No color change was observed in a control experiment with particles lacking biotin, confirming that assembly was

[1]Department of Chemistry, University of California, Berkeley and Materials Sciences Division, Lawrence Berkeley National Laboratory, Berkeley, California 94720, USA. [2]Department of Physics, University of California, Berkeley and Physical Biosciences Division, Lawrence Berkeley National Laboratory, Berkeley, California 94720, USA. [3]These authors contributed equally to this work. Correspondence should be addressed to J.L. (Liphardt@physics.berkeley.edu) or A.P.A. (alivis@berkeley.edu).

Published online 22 May 2005; doi:10.1038/nbt1100

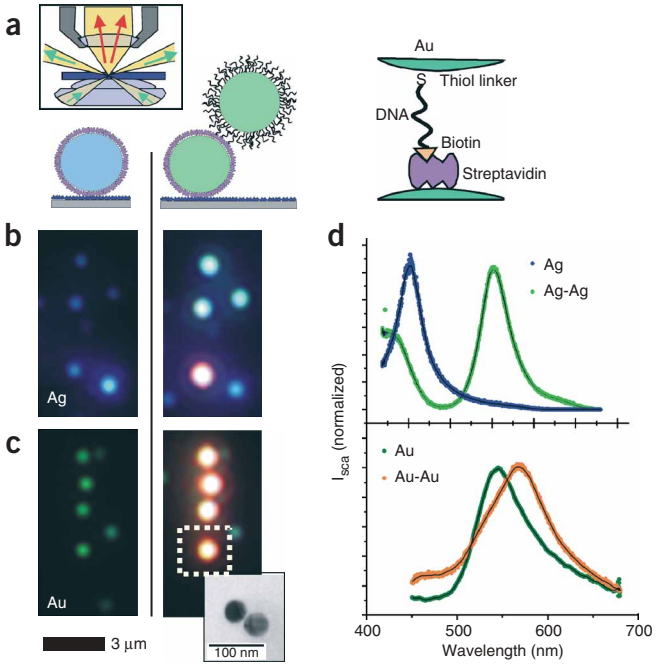

Figure 1 Color effect on directed assembly of DNA-functionalized gold and silver nanoparticles. (**a**) First, nanoparticles functionalized with streptavidin are attached to the glass surface coated with BSA-biotin (left). Then, a second particle is attached to the first particle (center), again via biotin-streptavidin binding (right). The biotin on the second particle is covalently linked to the 3′ end of a 33 base pair long ssDNA strand bound to the particle via a thiol group at the 5′ end. Inset: principle of transmission darkfield microscopy. (**b**) Single silver particles appear blue (left) and particle pairs blue-green (right). The orange dot in the bottom comes from an aggregate of more than two particles. (**c**) Single gold particles appear green (left), gold particle pairs, orange (right). Inset: representative transmission electron microscopy image of a particle pair to show that each colored dot comes from light scatted from two closely lying particles, which cannot be separated optically. (**d**) Representative scattering spectra of single particles and particle pairs for silver (top) and gold (bottom). Silver particles show a larger spectral shift (102 nm) than gold particles (23 nm), stronger light scattering and a smaller plasmon line width. Gold, however, is chemically more stable and is more easily conjugated to biomolecules via –SH, –NH2 or –CN functional groups.

directed by streptavidin/biotin. The two-particle complexes were stable and could be continuously monitored for hours. We routinely recorded their spectra for 3,000 s at 0.5 Hz. The connection axis of the particle dimer was randomly oriented in space as judged by the polarization of the scattered light.

Having established that particle pairs linked by ssDNA could be assembled on surfaces, we investigated whether DNA-linked nanoparticle pairs could be used to report the interparticle distance, *r*. As with many other rulers, macroscopic or microscopic, the observable for the plasmon ruler (the spectral shift) must be converted to a distance using either empirical calibration or an established physical theory. In the absence of an experimental study, we used a published spectral shift distance relationship $\Delta\lambda(r)$ obtained by solving the electrodynamic Maxwell equation for gold particles with 40 nm diameter in a dielectric medium (ref. 17, see Fig. 3a therein). Caution is required in applying these theoretical values to our system because there are unknown influences, such as the glass surface and the undefined orientation of our dimers, but for the current discussion, the above-mentioned relationship is sufficient.

As a first qualitative test of the plasmon ruler, we changed the interparticle distance by adjusting the ionic strength of the solution. The Debye screening length is larger in low salt concentrations, which should increase the electrostatic repulsion between the charged gold particles[26]. Consistent with this model, a blue-shift in the spectrum of individual nanoparticle pairs occurred when we decreased the salt concentration of our buffer (normally 0.1 M NaCl) to 0.005 M NaCl (**Fig. 2a**). When we restored the ionic concentration to the original value, we observed a red-shift. An effect due to a change in the refractive index was ruled out by observing nanoparticle pairs formed simply by precipitation. Such random particle pairs, not linked by DNA and unable to move relative to each other, showed no detectable spectral shift at salt concentrations between 0 and 0.1 M NaCl (data not shown).

For DNA-tethered particles, the observed shifts induced by buffer exchange were reversible, although not fully: the salt-dependent shifts were superimposed on a background red-shift of the spectrum, which was caused by flushing the chamber (**Fig. 2a**). The most likely explanation of this background red-shift is leaching of weakly bound ssDNA from the surface of the particles, which reduces their repulsive steric interactions. The possibility that additional DNA tethers gradually formed was excluded in a control experiment by blocking all free streptavidin sites with excess free biotin after formation of the initial complex, which left the red-shift unaffected. It is important to note that the gradual red-shift was observed only when the chamber was flushed with buffer. As long as the DNA-tethered particles were incubated in buffer without flushing, the plasmon wavelength remained constant (**Fig. 2b**). We found that this red-shift could be avoided altogether by attaching the DNA to the particles via linker molecules (biotin-neutravidin or digoxigenin–anti-digoxigenin; see **Supplementary Fig. 1a** online). These linker molecules serve as

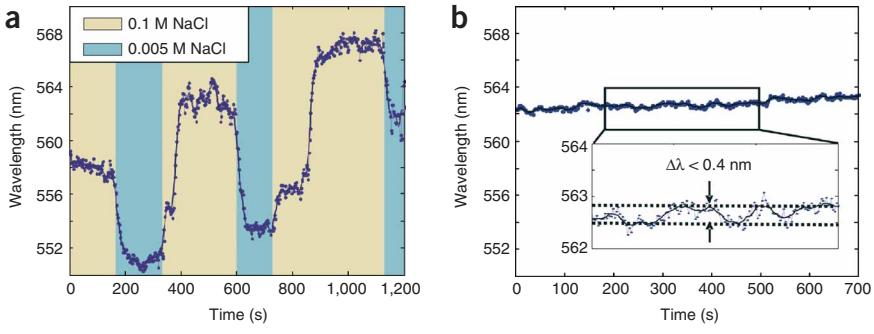

Figure 2 Effect of buffer exchange. (**a**) Peak wavelength of the plasmon resonance of a particle dimer when flushed with different salt concentrations (0.1 M NaCl and 0.005 M NaCl. The plasmon resonance shifts red with higher salt concentration, indicative of a decreased interparticle distance. This is due to the reduced electrostatic repulsion of the particles in high ionic strength environment. The Debye screening length is reduced from 4 nm to 1 nm. A gradual overall red-shift is also observed. (**b**) Without flushing, the peak wavelength of the plasmon resonance remains stable within 0.4 nm over 700 s.

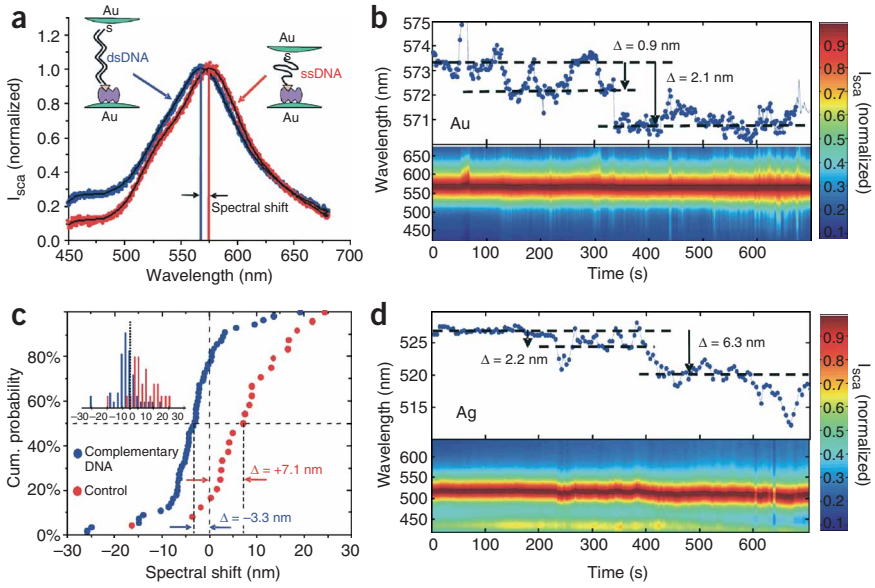

Figure 3 Spectral shift upon DNA hybridization. (**a**) Example of a spectral shift between a gold particle pair connected with ssDNA (red) and dsDNA (blue). The shift is clearly visible. (**b**) Spectral position as a function of time after addition of complementary DNA. The scattered intensity (Isca) is shown color-coded on the bottom; the peak position obtained by fitting each spectrum is traced on the top. Discrete states are observed, indicated by horizontal dashed lines. (**c**) Cumulative probability distribution of the spectral shift for ~80 particles induced by adding complementary DNA (blue) and noncomplementary DNA (red). Inset: histogram of the observed spectral shift. A student's *t*-test on this data proves the difference between experiment and control to be statistically significant ($P < 0.0001$). (**d**) Time dynamics for a silver particle dimer after addition of complementary DNA. The random fluctuations in the time traces due to solution effects and Brownian motion could be used to gain insight into the interparticle potential.

spacers to prevent the particles from coming into close range, where the attractive van der Waals interaction starts to dominate.

If the nanoparticle pairs were in fact acting as molecular rulers capable of reporting distance changes within one molecule, we reasoned that it should be possible to detect the hybridization of complementary DNA oligonucleotides to the ssDNA linkers. We chose double-stranded DNA (dsDNA) because it is well understood theoretically and extensively characterized experimentally. Indeed, we found a significant blue-shift upon addition of complementary DNA (**Fig. 3a**), indicative of hybridization. As dsDNA is much stiffer than ssDNA[22], the particles are pushed apart (inset, **Fig. 3a**). To record the dynamics of the DNA hybridization, we monitored the spectrum of single gold particle pairs continuously in time. A representative time trace is shown in the bottom panel of **Figure 3b**. We extracted the spectral peak position (top panel, **Fig. 3b**) by fitting the smoothed spectral data. These time traces reveal initial discrete on/off events with a spectral amplitude of $\Delta\lambda = 0.9$ nm. The subsequent larger, irreversible annealing step led to a total blue-shift of $\Delta\lambda = 2.1$ nm. Most likely, we were observing consecutive attachment/detachment of ssDNA complements to the DNA strand on the nanoparticle, which was eventually followed by the complete zipping of the helix to yield a duplex. The sudden spectral jumps strongly indicate that the signals originate from single molecules. To confirm the assignment of the spectral shifts as single DNA hybridization events, we converted the recorded spectral shifts to particle separations[17]. The spectral steps shown in **Figure 3b** correspond to a change in distance of $\Delta r = 0.8$ nm and $\Delta r = 2$ nm. The total change in length of 2 nm upon duplex formation agrees well with the change in DNA length of 1.9 nm upon hybridization predicted by the worm-like chain model[27] (32-nucleotide ssDNA, persistence length (p) = 2.0 nm, contour length (l) = 20.8 nm; 32-base-pair dsDNA, $p = 53$ nm, $l = 10.9$ nm).

Hybridization reactions of surface-immobilized DNA typically proceed in a series of consecutive steps. First, ssDNA strands from solution diffuse into the vicinity of the immobilized strands, and bases on the complementary strands start to interact through attractive van der Waals forces and form hydrogen bonds. A DNA duplex forms in a rapid zipping motion after a certain number of base pairs have spontaneously formed a stable nucleus (see, for example, ref. 24). Our data indicate that for nanoparticle-bound oligomers, several attachment/detachment events are required before a stable nucleus is formed and zipping can occur. This is consistent with previous observations of relatively inefficient hybridization of nanoparticle-bound oligomers[28].

To verify that hybridization is indeed the reason for the observed blue-shift, we carried out control experiments recording the spectral positions before and after addition of complementary and noncomplementary DNA. To record the spectra of several particles in the same chamber, we had to take the initial spectrum before flushing with DNA. (This is different from the time traces discussed above, which were started after flushing the chamber with DNA.) A clear difference between addition of complementary and noncomplementary DNA was visible (**Fig. 3c**). On average, addition of complementary DNA led to a blue-shift of $\Delta\lambda = 3.3$ nm, consistent with a hybridization-induced increase of interparticle spacing. The control shows an average red-shift of $\Delta\lambda = 7.1$ nm, caused by the flushing and stripping of ssDNA from the gold, as seen before in the salt-exchange experiment. The average blue-shift observed for DNA hybridization (3.3 nm) is larger than the shift observed in time traces on single-particle dimers (~2 nm). In the latter, we used DNA-conjugated nanoparticles with a low concentration of biotinylated DNA to increase the probability of a single tether, whereas the particles in the control experiment carried a higher number of biotinylated DNA molecules to increase the binding efficiency. We also recorded some DNA hybridization dynamics with dimers of 40-nm silver particles (**Fig. 3d**). As seen before (**Fig. 1d**), the plasmon coupling between silver particles led to a more pronounced spectral shift. Our explanation that DNA hybridization is responsible for the observed blue-shift via an increase in steric repulsion between the particles is further supported by the observation that addition of DNA-binding dendrimers leads to a drastic red-shift consistent with DNA wrapping around the dendrimer (see **Supplementary Fig. 1b** online).

Plasmon rulers have several key advantages over rulers based on Förster Resonance Energy Transfer (FRET) and should allow a wide range of new *in vitro* single-molecule experiments. In FRET, the fluorescence intensities of a donor-acceptor dye pair are monitored simultaneously. Only a distance change between the donor and acceptor results in an anticorrelated intensity change, whereas most other environmental effects lead to uncorrelated intensity changes. Unfortunately, observation of single-molecule fluorescence is hindered by blinking and

rapid photobleaching, limiting the continuous observation time to a few tens of seconds. Furthermore, it is sometimes difficult to distinguish changes in relative dye orientation from changes in distance[1].

The plasmon ruler neither blinks nor bleaches and does not depend on the relative probe orientation. Moreover, metal nanoparticles are good labels for electron and X-ray microscopy, which permits the development of novel multimodal imaging techniques. In general, gold and silver particles are more stable under physiological conditions than organic dyes. However, the plasmon resonance also depends on the refractive index of the surroundings. Especially in the case of small red-shifts it can be difficult to distinguish variations in the refractive index from distance changes, so the refractive index must be carefully controlled.

As in FRET, deducing absolute distances is complex. Experimental data on the distance dependence of plasmon coupling are limited, and the plasmon wavelength varies between particles of the same batch owing to variation in their shape and size. It is, however, conceivable that these limitations will be overcome. For instance, the lifetime of gold particles is nearly unlimited, which permits their characterization before or after use in a plasmon ruler. The range of distances accessible with plasmon coupling in a pair of nanoparticles depends on the size and coating of the particles. In general, the accessible distance range is larger than with FRET (2–8 nm)[1]. With 40-nm particles and a 0.1-nm spectral resolution for determining the plasmon resonance position, particle separations of up to 70 nm should be accessible with better than 1-nm resolution[17]. Larger particle separations, up to 2.5 times the particle diameter, still lead to some small shift in the plasmon resonance[18].

As light-scattering efficiency scales with the square of particle volume, it is difficult to use particles with diameters much smaller than 20–30 nm. The particles are therefore larger than the dyes used in conventional FRET-based molecular rulers. This is a disadvantage, especially for *in vivo* applications. However, most single-molecule studies have been performed *in vitro*, where the large particle size is not a fundamental limitation. Even micron-sized magnetic and polystyrene beads have been successfully used in single-molecule applications[23,29]. Another problem of plasmon-based rulers is the potential denaturing of proteins near metal surfaces. The routine use of antibody-coated gold nanoparticles as specific staining reagents in electron microscopy suggests that this problem can be avoided in most cases by using an appropriate spacer molecule.

Therefore, plasmon rulers have the potential to become an alternative to FRET for *in vitro* single-molecule experiments, especially for applications demanding long observation times or large distances. In addition, analytical bulk assays based on particle aggregation can now be extended to the single-molecule level, enhancing their sensitivity and allowing parallel processing. For example, extremely small numbers of DNA molecules, such as the unamplified genomic DNA of a single cell, should be detectable by incorporating plasmon rulers into a microfluidic system.

METHODS

General methods. Aqueous solutions of 40 nm gold and silver nanoparticles (British Biocell International, size deviation <10%) with a concentration of 9.0×10^{10} particles/ml $\approx 1.5 \times 10^{-10}$ M were purchased from Ted Pella. Deionized water (>18.0 MΩ) from a Barnstead D4641 water purification system was used for all experiments. All buffers were filtered with a 0.45 μm pore-size Millex-HA microfilter (Millipore) before use. Immediately after conjugation, the particles were immersed in storage buffer and stored at 4 °C for up to one month.

Preparation of nanoparticle conjugates of streptavidin. Streptavidin (Molecular Probes, S-888) was dissolved in T50 buffer (10 mM Tris, pH 8.0 and 50 mM NaCl) at a concentration of 1 mg/ml. We added 250 μl of this streptavidin solution to 10 ml of aqueous nanoparticle solution. After mixing thoroughly, we added 100 μl of 1.0 M $NaHCO_3$ to the reaction mix, which was then allowed to react for 10 min. Subsequently 50 μl of a 2% polyethylene glycol 6000 (Merck, 807491) solution was added and the reaction mixture was centrifuged at 800*g* for 35 min. The pellets were redissolved in Superblock (Pierce, 37515) and washed with Superblock using Microcon YM-100 centrifugal filter devices.

Preparation of DNA-functionalized nanoparticles. All DNA oligomers were purchased from Fidelity Systems. We used 3′ biotinylated ssDNA oligomers with a 5′ thiol modification ($OPO_3(CH_2)_6$-S-S-$(CH_2)_6OH$) and controls that were not biotinylated. The following sequences were used in our experiments:

A: (SS C6 linker) 5′-ACATTAAAATTCCACACACGCTAACATACACA-3′ (Biotin)T

B: (SS C6 linker) 5′-ACATTAAAATTCCACACACGCTAACATACACAT-3′

Our strategy to functionalize nanoparticles with thiol-modified oligonucleotides followed a published procedure[30]. The gold nanoparticles were derivatized with modified ssDNA oligomers by incubating 600 μl of gold nanoparticle solution overnight with 10 μl of a 100 μM solution of the disulfide-protected, biotinylated oligonucleotide in 10 mM Tris (pH 7.0). We added 5 μl of 5 M NaCl and 50 μl of 50 mM sodium phosphate buffer (pH 7.0) to the reaction mix. After 12 h another 5 μl of 5 M NaCl and 50 μl of 50 mM sodium phosphate buffer (pH 7.0) was added to a final concentration of 0.07 M NaCl and 7 mM sodium phosphate buffer. The reaction mix was then allowed to react for 48 h after which the volume was slowly reduced in vacuum to 250 μl within 48 h. Unbound oligonucleotides were subsequently removed by centrifugation and resuspension of the pellet (7,000*g*, twice). In the case of silver nanoparticles 600 μl solution was incubated overnight with 10 μl of 100 μM ssDNA solution. Then the NaCl and sodium phosphate buffer concentration was slowly adjusted to 0.07 M NaCl and 7 mM sodium phosphate buffer by adding 2.5 μl 5 M NaCl and 25 μl 50 mM sodium phosphate buffer (pH 7.0) every 24 h for a total of 96 h. After further incubation of 24 h the volume was slowly reduced to 250 μl within 48 h. Unbound DNA was removed by centrifugation (7,000*g*, once) and resuspension of the pellet. DNA-coated gold and silver nanoparticles were stored in a storage buffer (100 μl) containing NaCl (0.1 M) and sodium phosphate buffer (10 mM, pH 7.0). The zeta potential of the functionalized particles was determined to be −40 meV.

Surface immobilization of ssDNA-linked nanoparticle dimers. All attachment chemistry was conducted within a hollow rectangular glass capillary (Vitrocom) that served as flow chamber. The chamber had the dimensions (height × width × length) 0.1 mm × 1.00 mm × 100 mm and a wall thickness of 0.1 mm. Biotin-BSA (Sigma, A8549) was dissolved in T50 buffer to a total concentration of 1 mg/ml, and 100 μl was flowed into the chamber and allowed to incubate for 15 min after which the chamber was washed with 200 μl of deionized water. Then 50 μl of a 1:500 dilution of nanoparticle conjugate of streptavidin in storage buffer was added to the chamber and incubated for 2 min. Next, the chamber was washed with 300 μl storage buffer. Eventually 50 μl of a 1:10 dilution of DNA-derivatized nanoparticles in storage buffer was flowed into the chamber and incubated for 20 min. Then the chamber was washed again with storage buffer.

Solid-phase hybridization experiments. We mixed 25 μl of a 100-μM solution of target ssDNA—oligonucleotides complementary to the probe ssDNA linking the nanoparticles—in 10 mM Tris (pH 7.0) with 25 μl of hybridization buffer, which contained 20% formamide (Aldrich, F7508), 16% dextran sulfate (Aldrich, D6924) and 1 mM $MgCl_2$ (Ambion, #9530G) and incubated for up to an hour. Afterwards the chamber was washed with storage buffer. In control experiments the target ssDNA was replaced by noncomplementary ssDNA. The following sequences were used in the hybridization and control experiments:

C: 5′-TGTGTATGTTAGCGTGTGTGGAATTTTAATGT-3′ (target ssDNA, complementary to sequence A)

D: 5′-AGGTCGCCGCCCGCACAGTAGCGATTCAACGC-3′ (control)

Experimental setup. The darkfield optical setup consists of a 100 W tungsten lamp, an oil immersion darkfield condenser and a 40× objective. The scattered light was analyzed by a CCD camera cooled by liquid nitrogen and attached to an imaging spectrometer[25].

Calculation of refractive index effect. On random dimer pairs formed by precipitation of gold and silver particles on the glass surface, we measured the plasmon peak in water ($n = 1.333$), dimethylsulfoxide (DMSO, $n = 1.4782$) and mixtures of water and DMSO. The plasmon shift $\Delta\lambda$ increased linearly with refractive index change Δn. For $\Delta n = 0.1$ we obtained spectral shift $\Delta\lambda = 12.5$ nm for silver and $\Delta\lambda = 6.2$ nm for gold. The refractive index of salt solutions was proportional to the molar salt concentration with $\Delta n = 0.0091 \times$ [NaCl]. The range of buffers used in our experiments (0.005–0.1 M) therefore change the refractive index <0.001. The resulting spectral shift for gold dimers would amount to $<\Delta\lambda = 0.06$ nm. To account for the observed shift upon buffer exchange (**Fig. 2**) of 12 nm, the refractive index would have to change by $\Delta n = 0.2$, that is, from 1.33 to 1.53, well above that of most organic substances. This proves that the change in interparticle distance due to repulsion between the particles in low ionic strength environments indeed causes the observed shift.

Note: Supplementary information is available on the Nature Biotechnology website.

ACKNOWLEDGMENTS

We acknowledge financial support through the Alexander von Humboldt Foundation (C.S.), the Otto A. Wipprecht Foundation (B.M.R.), Deutsche Forschungsgemeinschaft (B.M.R.), US Department of Energy contracts DE-AC03-76SF00098 and W-7405-ENG-36.

COMPETING INTERESTS STATEMENT

The authors declare that they have no competing financial interests.

Received 2 March; accepted 25 April 2005
Published online at http://www.nature.com/naturebiotechnology/

1. Weiss, S. Fluorescence spectroscopy of single biomolecules. *Science* **283**, 1676–1683 (1999).
2. Zhuang, X. *et al.* A single-molecule study of RNA catalysis and folding. *Science* **288**, 2048–2051 (2000).
3. Yildiz, A. *et al.* Myosin V walks hand-over-hand: Single fluorophore imaging with 1.5-nm localization. *Science* **300**, 2061–2065 (2003).
4. Blanchard, S.C., Kim, H.D., Gonzalez, R.L., Puglisi, J.D. & Chu, S. tRNA dynamics on the ribosome during translation. *Proc. Natl. Acad. Sci. USA* **101**, 12893–12898 (2004).
5. Yguerabide, J. & Yguerabide, E.E. Light-scattering submicroscopic particles as highly fluorescent analogs and their use as tracer labels in clinical and biological applications - II. Experimental characterization. *Anal. Biochem.* **262**, 157–176 (1998).
6. Taton, T.A., Mirkin, C.A. & Letsinger, R.L. Scanometric DNA array detection with nanoparticle probes. *Science* **289**, 1757–1760 (2000).
7. Storhoff, J.J., Lucas, A.D., Garimella, V., Bao, Y.P. & Muller, U.R. Homogeneous detection of unamplified genomic DNA sequences based on colorimetric scatter of gold nanoparticle probes. *Nat. Biotechnol.* **22**, 883–887 (2004).
8. Li, H. & Rothberg, L. Colorimetric detection of DNA sequences based on electrostatic interactions with unmodified gold nanoparticles. *Proc. Natl. Acad. Sci. USA* **101**, 14036–14039 (2004).
9. Dragnea, B., Chen, C., Kwak, E.S., Stein, B. & Kao, C.C. Gold nanoparticles as spectroscopic enhancers for in vitro studies on single viruses. *J. Am. Chem. Soc.* **125**, 6374–6375 (2003).
10. Siedentopf, H. & Zsigmondy, R. Über Sichtbarmachung und Größenbestimmung ultramikroskopischer Teilchen, mit besonderer Anwendung auf Goldrubingläser. *Annalen der Physik* **10**, 1–39 (1903).
11. Mie, G. Beiträge zur Optik trüber Medien speziell kolloidaler Metallösungen. *Annalen der Physik* **25**, 377–445 (1908).
12. Moskovits, M. Surface-Enhanced Spectroscopy. *Rev. Mod. Phys.* **57**, 783–826 (1985).
13. Elghanian, R., Storhoff, J.J., Mucic, R.C., Letsinger, R.L. & Mirkin, C.A. Selective colorimetric detection of polynucleotides based on the distance-dependent optical properties of gold nanoparticles. *Science* **277**, 1078–1081 (1997).
14. McFarland, A.D. & Van Duyne, R.P. Single silver nanoparticles as real-time optical sensors with zeptomole sensitivity. *Nano Lett.* **3**, 1057–1062 (2003).
15. Raschke, G. *et al.* Biomolecular recognition based on single gold nanoparticle light scattering. *Nano Lett.* **3**, 935–938 (2003).
16. Kreibig, U. & Vollmer, M. Optical Properties of Metal Clusters **Vol. 25** (Springer-Verlag, Berlin, 1995).
17. Wei, Q.H., Su, K.H., Durant, S. & Zhang, X. Plasmon resonance of finite one-dimensional Au nanoparticle chains. *Nano Lett.* **4**, 1067–1071 (2004).
18. Su, K.H. *et al.* Interparticle coupling effects on plasmon resonances of nanogold particles. *Nano Lett.* **3**, 1087–1090 (2003).
19. Rechberger, W. *et al.* Optical properties of two interacting gold nanoparticles. *Opt. Commun.* **220**, 137–141 (2003).
20. Mirkin, C.A., Letsinger, R.L., Mucic, R.C. & Storhoff, J.J. A DNA-based method for rationally assembling nanoparticles into macroscopic materials. *Nature* **382**, 607–609 (1996).
21. Alivisatos, A.P. *et al.* Organization of 'nanocrystal molecules' using DNA. *Nature* **382**, 609–611 (1996).
22. Smith, S.B., Cui, Y.J. & Bustamante, C. Overstretching B-DNA: The elastic response of individual double-stranded and single-stranded DNA molecules. *Science* **271**, 795–799 (1996).
23. Singh-Zocchi, M., Dixit, S., Ivanov, V. & Zocchi, G. Single-molecule detection of DNA hybridization. *Proc. Natl. Acad. Sci. USA* **100**, 7605–7610 (2003).
24. Hagan, M.F. & Chakraborty, A.K. Hybridization dynamics of surface immobilized DNA. *J. Chem. Phys.* **120**, 4958–4968 (2004).
25. Sönnichsen, C. *et al.* Drastic reduction of plasmon damping in gold nanorods. *Phys. Rev. Lett.* **88**, 077402 (2002).
26. Park, S.J., Lazarides, A.A., Storhoff, J.J., Pesce, L. & Mirkin, C.A. The structural characterization of oligonucleotide-modified gold nanoparticle networks formed by DNA hybridization. *J. Phys. Chem. B* **108**, 12375–12380 (2004).
27. Tinoco, I. Force as a useful variable in reactions: Unfolding RNA. *Annu. Rev. Biophys. Biomol. Struct.* **33**, 363–385 (2004).
28. Demers, L.M. *et al.* A fluorescence-based method for determining the surface coverage and hybridization efficiency of thiol-capped oligonucleotides bound to gold thin films and nanoparticles. *Anal. Chem.* **72**, 5535–5541 (2000).
29. Itoh, H. *et al.* Mechanically driven ATP synthesis by F-1-ATPase. *Nature* **427**, 465–468 (2004).
30. Kanaras, A.G., Wang, Z.X., Bates, A.D., Cosstick, R. & Brust, M. Towards multistep nanostructure synthesis: Programmed enzymatic self-assembly of DNA/gold systems. *Angew. Chem. Int. Ed.* **42**, 191–194 (2003).